



The Cellular and Viral circRNAome Induced by Respiratory Syncytial Virus Infection

Wenxia Yao,^a Jinghui Pan,^a Zhaoyu Liu,^a Zhijie Dong,^a Min Liang,^a Shu Xia,^{b,c} Yao Xiao,^a Xiaodan Cai,^d Tao Peng,^b Xinke Zhou,^a Hua Cai^{a,b}

^aThe Fifth Affiliated Hospital of Guangzhou Medical University, Guangzhou Medical University, Guangzhou, China

^bGuangzhou Hoffmann Institute of Immunology, College of Basic Sciences, Guangzhou Medical University, Guangzhou, China

^cThe First Affiliated Hospital of Guangzhou Medical University, Guangzhou Medical University, Guangzhou, China

^dGuangzhou Gene Denovo Biotechnology Co. Ltd., Guangzhou, China

Wenxia Yao, Jinghui Pan, and Zhaoyu Liu contributed equally to this article. Author order was determined based on seniority.

ABSTRACT Circular RNAs (circRNAs) are a new class of noncoding RNAs that have gained increased attention. DNA virus infections have been reported to induce modifications in cellular circRNA transcriptomes and express viral circRNAs. However, the identification and expression of cellular and viral circRNAs are unknown in the context of respiratory syncytial virus (RSV), a human RNA virus with no effective treatments or vaccines. Here, we report a comprehensive identification of the cellular and viral circRNAs induced by RSV infection in A549 cells with high-throughput sequencing. In total, 53,719 cellular circRNAs and 2,280 differentially expressed cellular circRNAs were identified. Trend analysis further identified three significant expression pattern clusters, which were related to the antiviral immune response according to gene enrichment analysis. Subsequent results showed that not only RSV infection but also poly(I-C) treatment and another RNA virus infection induced the upregulation of the top 10 circRNAs from the focused cluster. The top 10 circRNAs generally inhibit RSV replication in turn. Moreover, 1,254 viral circRNAs were identified by the same circRNA sequencing. The induced expression of viral circRNAs by RSV infection was found not only in A549 cells but also in HEP-2 cells. Additionally, we profiled the general characteristics of both cellular and viral circRNAs such as back-splicing signals, etc. Collectively, RSV infection induced the differential expression of cellular circRNAs, some of which affected RSV infection, and RSV also expressed viral circRNAs. Our study reveals novel layers of host-RSV interactions and identifies cellular or viral circRNAs that may be novel therapeutic targets or biomarkers.

IMPORTANCE Noncoding RNAs (ncRNAs) demonstrate substantial roles in cell-virus interactions. Circular RNAs (circRNAs) are a newly identified class of ncRNAs that have gained increased attention recently. DNA virus infections have been reported to induce modifications in cellular circRNA transcriptomes and express viral circRNAs. However, the identification and expression of cellular and viral circRNAs are unknown in the context of respiratory syncytial virus (RSV), a human RNA virus with no effective treatments or vaccines. Here, we report a comprehensive identification of the cellular and viral circRNAs induced by RSV infection by high-throughput sequencing. We revealed that RSV infection induces the differential expression of cellular circRNAs, some of which affected RSV infection, and that RSV also expresses viral circRNAs. Our study reveals novel layers of host-RSV interactions and identifies cellular or viral circRNAs that may be novel therapeutic targets or biomarkers.

KEYWORDS RSV, cellular circRNAs, viral circRNAs, antiviral immune response

Invited Editor Erik K. Flemington, Tulane University Health Sciences Center and Tulane Cancer Center

Editor Christine A. Biron, Brown University

Copyright © 2021 Yao et al. This is an open-access article distributed under the terms of the [Creative Commons Attribution 4.0 International license](https://creativecommons.org/licenses/by/4.0/).

Address correspondence to Wenxia Yao, yaowenxia917@126.com, Xinke Zhou, zxkstar@126.com, or Hua Cai, chjorbe@hotmail.com.

Received 15 October 2021

Accepted 29 October 2021

Published 7 December 2021

Respiratory syncytial virus (RSV) is a nonsegmented RNA virus that belongs to the genus *Pneumovirus* of the family *Paramyxoviridae* (1). Similar to other negative-strand RNA viruses, the RSV genome is a template for two processes, namely, transcription that yields mRNAs and replication that yields an antigenome RNA; the antigenome, in turn, acts as a template for genome synthesis. RSV infection occurs in over 95% of humans by 2 years of age and recurs throughout life. RSV infection can result in serious respiratory symptoms in infants and the elderly, and it is one of the leading causes of infant mortality worldwide (second only to malaria) (2). Treatment strategies for RSV infection are limited to palivizumab, which is a costly monoclonal antibody that is approved only for prophylaxis in high-risk infants, and ribavirin, which has limited efficacy and entails serious safety concerns (3). Despite substantial effort, including the preclinical or clinical development of various vaccine candidates, a safe, effective, clinically approved RSV vaccine has not been developed to date (4, 5).

Eukaryotic cells produce several classes of noncoding RNAs (ncRNAs), and circular RNAs (circRNAs) are a newly identified class of ncRNAs that have recently elicited increased attention (6–8). circRNAs are formed by the back-splicing of a downstream splice donor site to an upstream splice acceptor site, thus producing a covalently closed RNA molecule with no 5' caps or 3' poly(A) tails. circRNAs are unusually stable, presumably because their lack of free ends is resistant to exonuclease activity, which enables circRNAs to serve as a new class of potential biomarkers. Although our understanding of the functions of circRNAs is still nascent, an increasing number of studies have shown that circRNAs can sequester microRNAs or proteins, modulate transcription, interfere with splicing, and even translate to produce polypeptides or proteins (9). Furthermore, emerging lines of studies have revealed that some circRNAs play important roles under physiological and pathological conditions, and they may serve as diagnostic or predictive biomarkers of diseases and provide new potential therapeutic targets (10).

Viral infections can induce modifications in cell transcriptomes, including the circRNA transcriptome. Shi et al. and Tagawa et al. have respectively reported that infections by the human DNA viruses herpes simplex virus (HSV) and Kaposi's sarcoma-associated herpesvirus (KSHV) induce changes in cellular circRNA transcriptomes (11, 12). As virus hosts, eukaryotic cells rely on their innate immune response as the first line of defense against viruses. Similar to their host cells, many viruses synthesize their own viral ncRNAs, and multiple biological roles, including the regulation of viral replication or persistence and host immune evasion, have been ascribed to viral ncRNAs (13). Several research teams discovered and validated the presence of viral circRNAs in DNA viruses (14, 15) such as Epstein-Barr virus (EBV) and KSHV with large genomes (16–18) and human papillomaviruses (HPVs) with small genomes (19). In addition, Cai et al. predicted some circRNAs in RNA viruses by systematic bioinformatics analysis of the viral infection-related RNA sequencing (RNA-seq) data (20).

However, the identification and characterization of cellular and viral circRNAs are unknown in the context of RSV, a human RNA virus with no effective treatments or vaccines: whether or not the expressions of cellular circRNAs are regulated by RSV infection and subsequently affect RSV infection and whether there are viral circRNAs derived from RSV remain unclear. In the present study, we performed a comprehensive identification and expression analysis of cellular and viral circRNAs induced by RSV infection in A549 cells. We revealed novel cell-virus interactions of circRNAs: cellular circRNAs were induced in response to RSV infection and potentially affected RSV infection, and RSV could also express viral circRNAs.

RESULTS

Identification and profiling of cellular circRNAs in mock- and RSV-infected A549 cells. To characterize circRNA transcripts, we performed RNA sequencing (RNA-seq) analysis of rRNA-depleted and RNase R-treated total RNA isolated from A549 cells infected with RSV at 24 and 48 h, with mock-infected A549 cells as a negative group (Fig. 1A). The multiplicity of infection (MOI) was 1, and each group had two repetitive samples. As shown, RSV-infected A549 cells showed an apparent cytopathic effect,

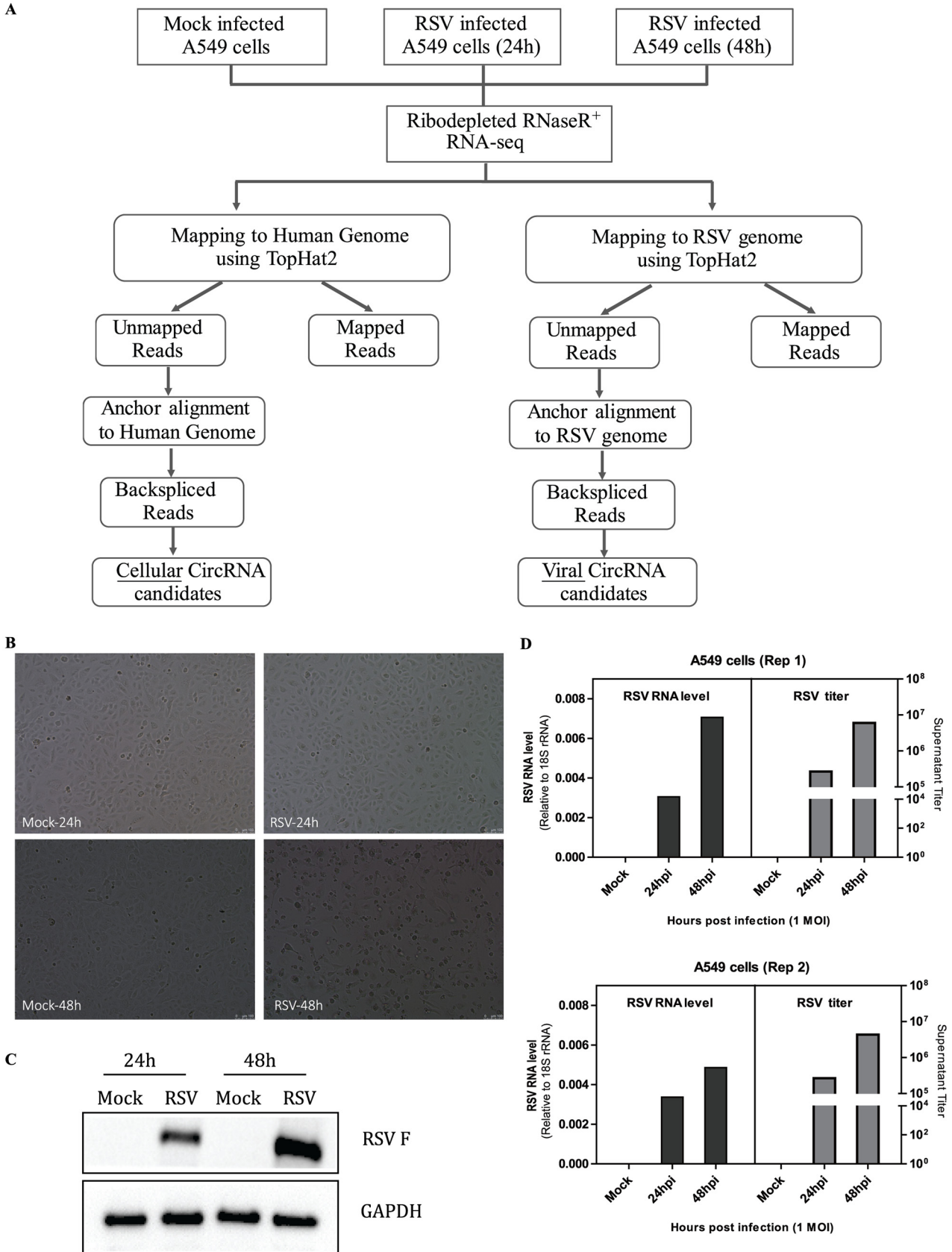


FIG 1 Experimental schema for the identification of cellular and viral circRNA candidates in mock- and RSV-infected A549 cells and characterization of mock and RSV infection in A549 cells. (A) Flowchart demonstrating how the high-throughput sequencing data were analyzed (Continued on next page)

TABLE 1 Summary of RNA-seq data sets from mock- and RSV-infected A549 cells^a

Sample	Total no. of reads	Mapping ratio to human genome (%)	No. of cellular circRNAs	Mapping ratio to RSV genome (%)	No. of viral circRNAs
Mock_Rep1	106,966,198	92.35	25,609	0.00	0
RSV-24h_Rep1	103,175,460	91.98	25,445	0.67	35
RSV-48h_Rep1	106,871,262	86.14	26,455	6.10	906
Mock_Rep2	97,770,190	92.55	24,726	0.00	0
RSV-24h_Rep2	102,777,188	92.03	25,102	0.39	46
RSV-48h_Rep2	104,870,684	89.30	25,523	3.30	688
Total			53,719		1,254

^aThe human genome was GRCh38; the GenBank nucleotide sequence accession no. of the RSV genome is [M74568.1](#). Mock, mock infected cells. RSV-24h, RSV infected cells (24h). RSV-48h, RSV infected cells (48h). Rep 1, repetitive sample 1. Rep 2, repetition sample 2.

especially at 48 h (Fig. 1B), and RSV F protein expression (Fig. 1C); moreover, RSV-infected A549 cells demonstrated robust RSV RNA expression and virus production (Fig. 1D). Each sample was sequenced on an Illumina HiSeq 2500 instrument, and >15 billion bases of data were produced. The obtained reads, which were filtered residual rRNA reads, were mapped to the human reference genome (GRCh38) and the RSV genome (GenBank nucleotide sequence accession no. [M74568.1](#)) by TopHat2 (Fig. 1A). Next, the unmapped reads were extracted, and a computational pipeline based on anchor alignment was implemented to identify cellular and viral circRNAs (Fig. 1A). Briefly, 20-mers from both ends of the unmapped reads were extracted and aligned to the reference human or RSV genome to determine unique anchor positions. Anchor reads that aligned in the reverse orientation indicated circRNA back-splicing and were then subjected to find_circ (6) to identify circRNAs (Fig. 1A). A candidate circRNA was called when it was supported by at least two unique back-splicing reads. A detailed summary of the RNA-seq data sets for each sample is provided in Table 1.

In total, 53,719 distinct cellular circRNA candidates were identified by this approach (Fig. 2A); 15,700 of them were matched in circBase (21), and 38,019 of them were novel circRNAs. The circRNA distributions of each group on human chromosomes showed that circRNAs were widely distributed among all chromosomes, including sex chromosomes, with the largest number of circRNAs on chromosomes 1 and 2 and the smallest number on chromosome Y (see Fig. S1A and B in the supplemental material). We then annotated the identified circRNA candidates using the RefSeq database (22). Approximately 78% of the circRNAs originated from coding DNA sequences (CDSs), whereas smaller fractions aligned with the 5' untranslated region (UTR), the 3' UTR, exon-introns, or antisense sequences (Fig. 2B). The average and median lengths of the cellular circRNAs were 2,386 and 637 nucleotides (nt), respectively (Fig. S1C). The splicing signals of the cellular circRNAs were also investigated, and the results indicated that most (93.4%) of the splicing signals had a canonical GT/AG donor/acceptor sequence (Fig. 2C), which is consistent with the previously reported circRNAs in mammals (23).

Characterizing differentially expressed cellular circRNAs in mock- and RSV-infected A549 cells. circRNA expression in mock- and RSV-infected A549 cells was calculated based on RPM (back-splicing junction reads per million mapped reads), which permits quantitative

FIG 1 Legend (Continued)

and how cellular and viral circRNAs were identified. Briefly, each sample RNA was ribodepleted and treated with RNase R prior to library preparation, and each sample was sequenced using an Illumina HiSeq 2500 instrument. The obtained reads were mapped to the human genome and the RSV genome by TopHat2. Next, 20-mers from both ends of the unmapped reads were extracted and aligned with the human or RSV genome to determine unique anchor positions. Anchor reads that aligned in the reverse orientation indicated circRNA back-splicing and were subjected to find_circ to identify cellular or viral circRNAs. A candidate circRNA was called when it was supported by at least two back-splicing reads. Each group has two repetitive samples. (B to D) Characterization of RSV infection in A549 cells at 24 and 48 h, with mock infection as a negative group. (B) Induction of cytopathic effects in A549 cells. (C) Analysis of RSV F protein expression by Western blotting. (D) Analysis of intracellular RSV RNA levels by qRT-PCR and extracellular RSV titers by plaque assays in two repetitive samples. In panels A to D, the multiplicity of infection (MOI) was 1.

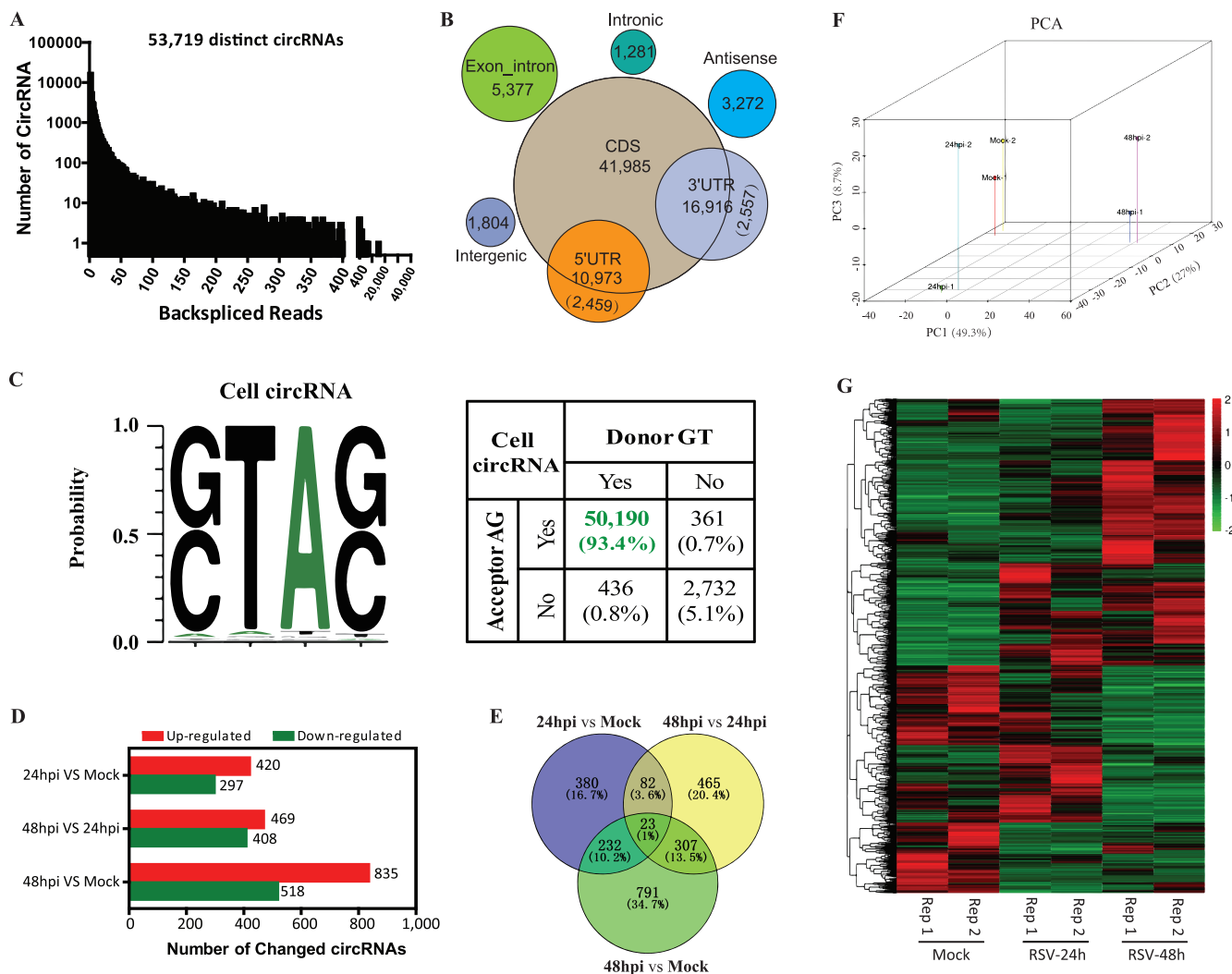


FIG 2 Profiling of cellular circRNAs and characterization of differentially expressed cellular circRNAs in mock- and RSV-infected A549 cells. (A) Numbers of cellular circRNAs and back-spliced reads identified in all samples. (B) Genomic region annotations and numbers of cellular circRNAs. (C) Back-splice signals of cellular circRNAs. (D) Bar plots demonstrating the numbers of differentially regulated circRNAs in each paired group. (E) Venn diagram presenting the number of differentially expressed circRNAs that are unique or common in each paired group. (F) Principal-component analysis (PCA) of the 2,280 differentially expressed cellular circRNAs. (G) Clustered heat map for the 2,280 differentially expressed cellular circRNAs from all samples, with rows representing circRNAs and columns representing samples. The numerical data represent normalized log₁₀-transformed RPM.

comparisons. Filtering analysis by the criteria of a fold change (FC) of >2.0 or <0.5 and a *P* value of <0.05 identified 2,947 cellular circRNAs whose expression was differentially regulated among the three groups (Fig. 2D). The distributions and numbers of upregulated or downregulated circRNAs are shown in volcano plots (Fig. S1D) and bar charts (Fig. 2D), respectively. As shown in Fig. 2D, the RSV-infected group at 48 h postinfection (hpi) had the largest number of differentially regulated circRNAs, that is, 835 upregulated and 518 downregulated circRNAs, compared with the mock group; additionally, 469 upregulated and 408 downregulated circRNAs were identified when the RSV 48-hpi group was compared with the RSV 24-hpi group, and 420 upregulated and 297 downregulated circRNAs were identified when the RSV 24-hpi group was compared with the mock group.

Furthermore, a Venn diagram was plotted to display the differently and commonly regulated circRNAs, and the results showed that three groups shared 23 common differentially expressed circRNAs, with each paired group having 82, 232, and 307 commonly regulated circRNAs (Fig. 2E). Combining the data in Fig. 2D with those in Fig. 2E, there were in total 2,280 nonoverlapping differentially expressed circRNAs. Three-dimensional principal-component analysis (PCA) of the 2,280 differentially expressed circRNAs revealed that

each of the three groups could be separated from the other two groups by plotting the three largest sources of variance (PC1, PC2, and PC3) (Fig. 2F). Clustering analysis of the 2,280 differentially expressed circRNAs suggested different expression patterns of circRNAs in the three groups (Fig. 2G).

Identification of temporally expressed clusters with 2,280 differentially expressed circRNAs and further function enrichment analysis. To unveil the dynamically expressed RSV-associated circRNAs, we performed short time series expression miner (STEM) clustering (24). We obtained three significant temporal expression clusters ($P < 0.05$) (Fig. 3A to C) and five nonsignificant temporal expression clusters (Fig. S2) with the 2,280 differentially expressed circRNAs. Line plots and violin plots were used to show fold changes and RPM expression levels, respectively (Fig. 3A to C and Fig. S2). We found that the trend of the three significant clusters was generally rising, whereas that of the five nonsignificant clusters was descending (Fig. S2A) or nondirectional (Fig. S2B). We named the three significantly up-regulated clusters UP1, UP2, and UP3, which had 328, 237, and 524 circRNAs, respectively. Representative circRNAs of each cluster are listed in the bottom panels of Fig. 3A to C.

We next performed gene ontology (GO) and KEGG pathway enrichment analyses for parental protein-coding genes using DAVID (25). In the analysis, we focused on the three significant clusters with a total of 1,089 cellular circRNAs from 871 parental source genes. The top 41 regulated GO processes ($P < 0.01$) (Fig. 3D) and the top 21 regulated KEGG pathways ($P < 0.05$) (Fig. 3E) were demonstrated and ranked according to their P values. The 871 genes demonstrated significant enrichment of GO terms related to the type I interferon (IFN) signaling pathway, the interferon gamma-mediated signaling pathway, positive regulation of the RIG-I signaling pathway, the defense response to virus, the innate immune response, positive regulation of NF- κ B transcription factor (TF) activity, and viral process, etc. (Fig. 3D). They also demonstrated significant enrichment of KEGG pathways related to herpes simplex virus infection, Epstein-Barr virus infection, influenza A virus infection, the NF- κ B signaling pathway, and hepatitis C virus infection, etc. (Fig. 3E). In summary, GO and KEGG pathway enrichment analyses indicate that circRNAs may be related to the innate immune response, the interferon signaling pathway, and pathways related to virus infection.

Validation of the top 10 cellular circRNAs from the UP1 cluster and verification of their upregulation induced by RSV infection. For further analysis, we focused on the UP1 cluster circRNAs that exhibited a steady increase upon RSV infection. We selected the top 10 circRNAs and called them *RSV-stimulated circRNAs* (RSCs). Cutoff filtering for selection was as follows: a >3 -fold alteration of circRNA expression was demonstrated when the RSV 24-hpi group was compared with the mock group, and a >6 -fold alteration of circRNA expression was demonstrated when the RSV 48-hpi group was compared with the RSV 24-hpi group. Detailed characteristics and a heat map of the expression of the 10 RSCs are shown in Table 2 and Fig. 4A, respectively. Divergent primers (Table S1A) were designed against the 10 circRNAs. Each primer pair amplified a single, distinct product of the expected size from RSV-infected A549 cells (Fig. S3A), and back-splicing junctions were further validated by Sanger sequencing (Fig. S3B). The enrichment of the 10 back-spliced circRNAs was apparent following RNase R treatment, whereas the abundance of linear glyceraldehyde-3-phosphate dehydrogenase (GAPDH) RNAs decreased (Fig. 4B).

We next validated the high expression levels of the 10 RSCs induced by RSV infection (MOI = 1) via quantitative real-time PCR (qRT-PCR), and the induced expression tendency was consistent with the RNA-seq results (Fig. 4C). Three of the RSCs (RSC3, RSC4, and RSC5) were induced more than 20-fold upon RSV infection, and RSC5 was induced more than 100-fold (Fig. 4C).

Both poly(I-C) and another RNA virus also induced upregulation of the 10 RSCs from the UP1 cluster, and these RSCs generally inhibit RSV replication. circRNAs may be upregulated by the antiviral response induced by RSV infection, and the above-described GO and KEGG pathway enrichment analyses, which showed that parental genes may be related to the innate immune response and the interferon signaling pathway, also supported this assumption. Given that double-stranded RNA (dsRNA) regions of viral genomes or viral replication can be detected by antiviral sensors and induce the expression of IFN and

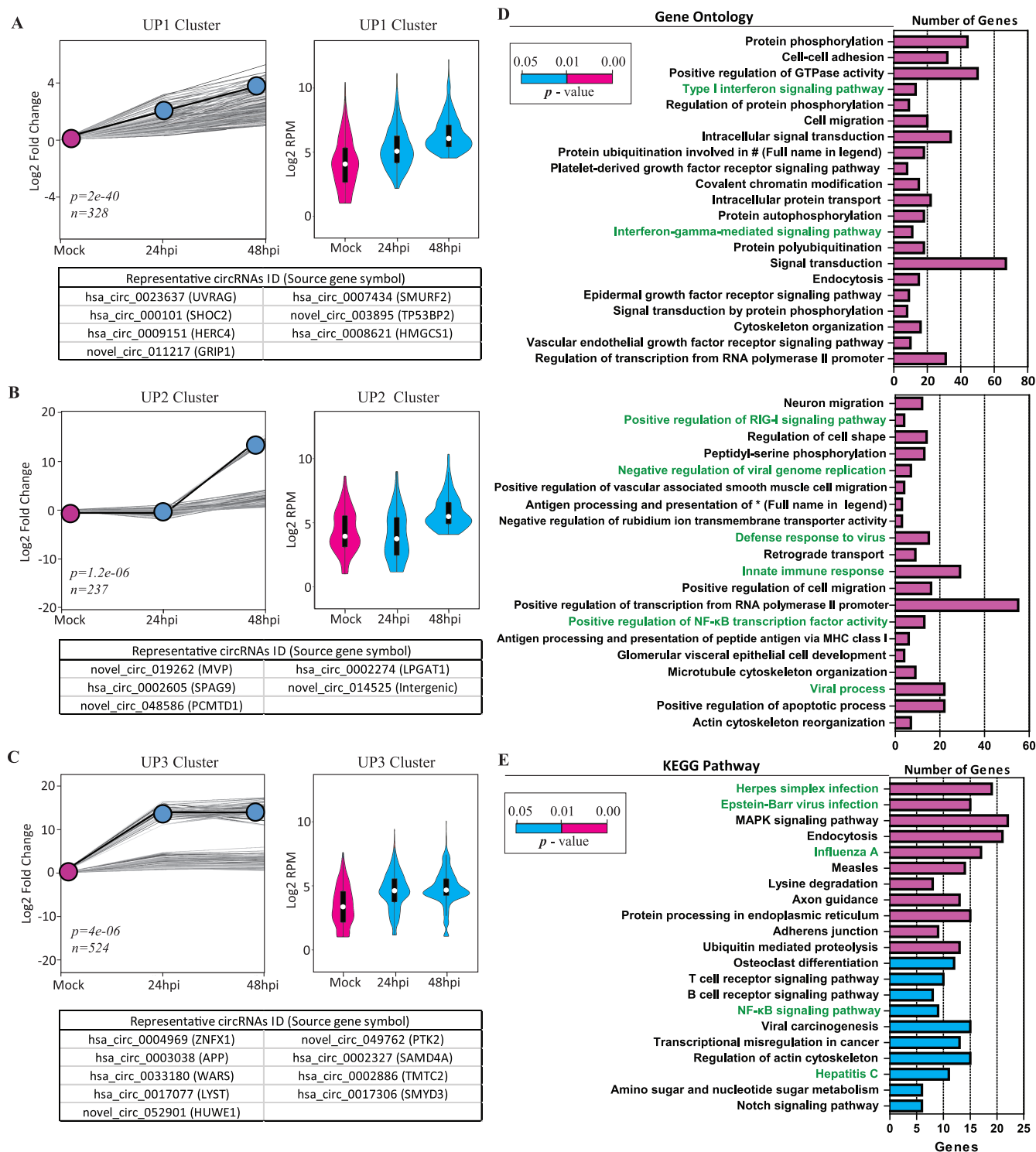


FIG 3 Trend analysis of temporally expressed clusters with 2,280 differentially expressed circRNAs and further GO and KEGG enrichment analyses of circRNAs from the three significant expression clusters. (A to C) Time series analysis of the 2,280 differentially expressed circRNAs with a 2-fold change in at least one time point. Results show three significant temporal clusters by STEM analysis ($P < 0.05$). (Left) Line plots were used to show fold changes (the number of circRNAs assigned to each cluster and P values are shown). The gray lines indicate the profiles of individual circRNAs, and the black lines show the model profile for each cluster in the line plots. (Right) Violin plots were used to show the absolute expression levels (\log_2 scale). (Bottom) Representative circRNAs with the source gene symbol in parentheses for each cluster. (D and E) GO (D) and KEGG pathway (E) enrichment analyses for parental protein-coding genes of circRNAs from the three significant temporal expression clusters. Enriched GO terms and KEGG pathways associated with virus infections and the immune response are indicated in green (#, ubiquitin-dependent protein catabolic process). MHC, major histocompatibility complex; MAPK, mitogen-activated protein kinase.

TABLE 2 List of circRNAs validated by divergent primers

circRNA	circBase ID	Positions ^a	Strand	Genomic length (bp)	Spliced length (bp)	Gene symbol
RSC1	hsa_circ_0025721	chr12: 27368262–27390239	+	21,978	888	ARNTL2
RSC2	hsa_circ_0001964	chr12: 27368262–27380404	+	12,143	453	ARNTL2
RSC3	hsa_circ_0004662	chr6: 159682474–159688242	–	5,769	462	SOD2
RSC4	hsa_circ_0082624	chr7: 139061036–139074030	–	12,995	399	ZC3HAV1
RSC5	hsa_circ_0001426	chr4: 88475841–88494331	+	18,491	1,052	HERC5
RSC6	hsa_circ_0003922	chr2: 230442937–230450255	+	7,319	713	SP100
RSC7	hsa_circ_0134778	chr7: 8003908–8071131	+	67,224	720	GLCC1
RSC8	hsa_circ_0008706	chr9: 110136127–110138539	+	2,413	2,413	PALM2-AKAP2
RSC9	hsa_circ_0007242	chr10: 13127745–13136897	+	9,153	523	OPTN
RSC10	hsa_circ_0082633	chr7: 139083780–139089759	–	5,980	389	ZC3HAV1
rsv_circ_449		RSV: 2348–2600	+	252	252	RSV P gene
rsv_circ_482		RSV: 2356–2597	+	241	241	RSV P gene
rsv_circ_664		RSV: 2879–3077	+	198	198	RSV P gene
rsv_circ_969		RSV: 5938–6921	+	983	983	RSV F gene
rsv_circ_305		RSV: 1571–1802	+	231	231	RSV N gene
rsv_circ_443		RSV: 2348–2580	–	232	232	RSV P gene
rsv_circ_526		RSV: 2368–2597	+	229	229	RSV P gene
rsv_circ_561		RSV: 2379–2605	+	226	226	RSV P gene

^achr, chromosome.

other antiviral genes, we investigated whether or not the dsRNA analogue poly(I:C) (pIC) could induce these RSCs' upregulation. The results showed that all of the top 10 RSCs were significantly increased after transfection of A549 cells with pIC (Fig. 4D), and the fold changes were similar to those induced by RSV infection (Fig. 4C and D). As circRNAs were induced by pIC treatment, we speculated that they might also be induced after infection with other RNA viruses. Therefore, we evaluated circRNA levels in A549 cells infected with vesicular stomatitis virus (VSV), an RNA virus that replicates in the cytoplasm, which is similar to RSV, at an MOI of 1. As shown in Fig. 4E, VSV also induced the upregulation of 10 RSCs detected 24 h after infection.

We then investigated the effect of the top 10 RSCs on RSV infection in turn, and the subcellular localization of the 10 RSCs was also analyzed. The effect of the 10 RSCs on RSV infection was explored using RNA interference. We designed small interfering RNAs (siRNAs) for each circRNA (Table S1A), with the exception of RSC2, which we failed to design due to the special back-splice sequence. All the designed siRNAs targeted the back-splice sequence and therefore did not affect the expression of parental linear genes. A549 cells were transfected with pooled siRNAs prior to infection with RSV and collected at 48 hpi; the previously reported siRNA ALN-RSV01, which is directed against the RSV N protein and reduces RSV replication both *in vitro* and *in vivo* (26, 27), was transfected as a control. As expected, ALN-RSV01 efficiently impaired the RSV RNA level (Fig. 5A), and the pooled RSC-specific siRNAs efficiently decreased the levels of the respective circRNAs (Fig. 5B). Under these conditions, the RSV RNA levels were significantly increased by silencing all nine circRNAs, and RSC5 showed the most significant effect (Fig. 5A). Next, subcellular localization was evaluated via qRT-PCR in nuclear or cytoplasmic fractions of RSV-infected cells. As expected, U1 snRNA was enriched in the nuclear fraction, while the coding GAPDH mRNA was preferentially enriched in the cytoplasm; as demonstrated, nearly all of the top 10 circRNAs accumulated preferentially in the cytoplasm, and only RSC10 accumulated in both the cytoplasm and nucleus (Fig. 5C). In summary, the nine cellular circRNAs from the UP1 cluster generally inhibited RSV replication.

Identification and profiling of viral circRNAs in RSV-infected A549 cells. Besides cellular circRNAs, we also investigated whether there are viral circRNAs derived from RSV. The pipeline used to identify cellular and viral circRNAs is illustrated in Fig. 1A. A total of 1,254 identified viral back-splice junctions of the RSV-infected samples were displayed using Integrative Genomics Viewer (IGV) (28) in reference to the RSV genome. The coverage depth is indicated on the y axis for each alignment panel (Fig. 6A). A total of 389 viral back-splice reads with high confidence, which were supported by

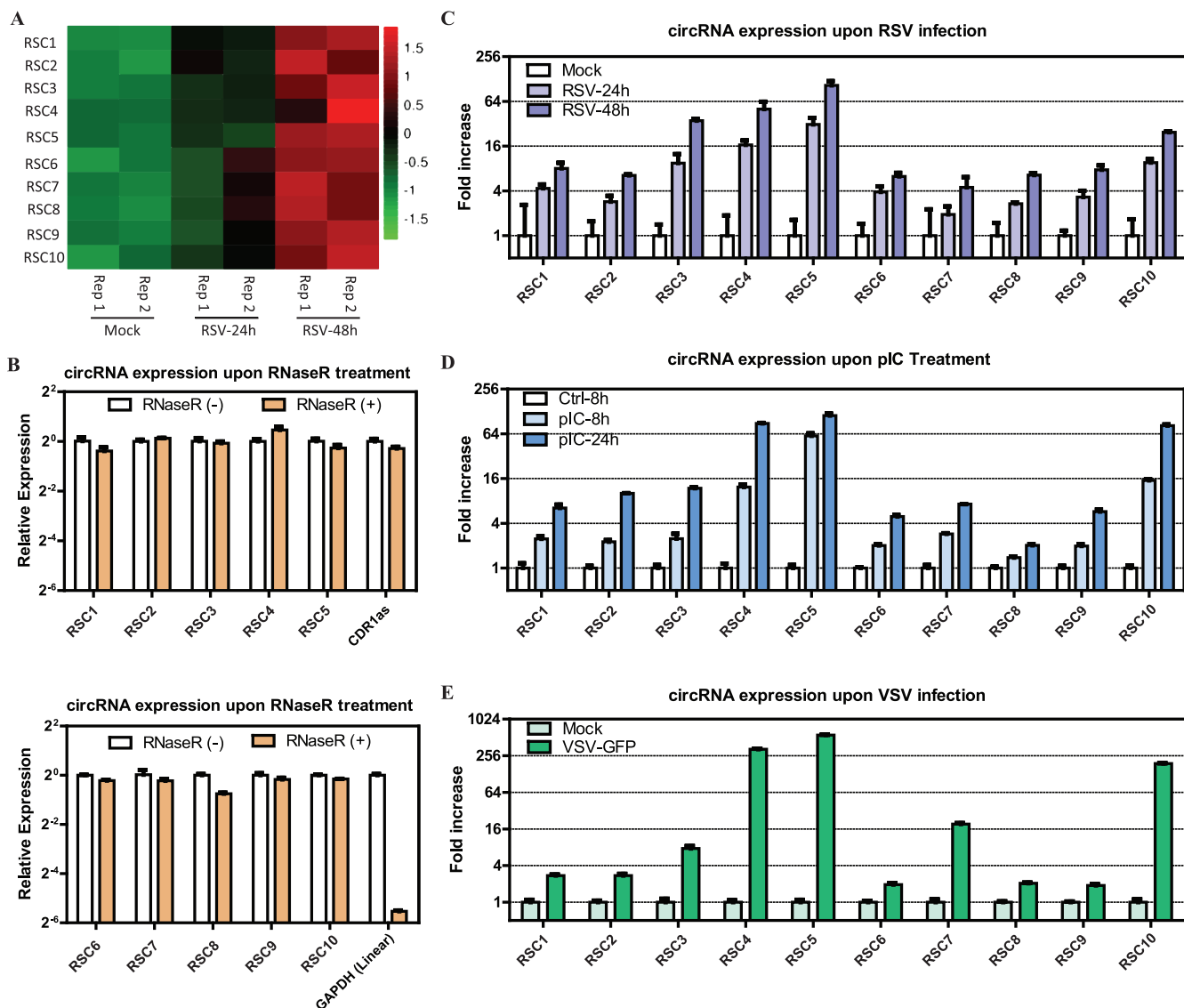


FIG 4 Validation of the top 10 RSCs from the UP1 cluster and effects of RSV infection, pIC, and VSV infection on the expression of the top 10 RSCs. (A) Heat map for the top 10 RSCs based on normalized RPM of RNA-seq data (\log_{10} scale). (B) qRT-PCR analysis of the abundances of cellular circRNAs treated with RNase R. The amounts were normalized to the value measured in the untreated group. (C) Effect of RSV infection (MOI = 1) on the expression of the top 10 RSCs by qRT-PCR analysis. The amounts were normalized to the value measured in the mock infection group. (D) Effect of pIC on the expression of the top 10 RSCs. (E) Effect of VSV-GFP (green fluorescent protein) infection (MOI = 1) on the expression of the top 10 RSCs. Data in panels B to E are presented as means \pm standard errors of the means (SEMs) ($n = 3$).

more than 5 reads in RSV-infected samples, are further demonstrated in Fig. S4. As shown in Fig. 6A and Fig. S4, apparent coverage peaks or high coverage densities were observed across the P, N, NS2, M, and F genes of the RSV genome. We also analyzed the number of circRNAs for each RSV gene from the general RSV RNA (1,254 in total), positive-sense RNA/mRNA (889 in total), and negative-sense RNA (365 in total), and the results showed that the P, F, N, M, and NS2 genes were the top five genes with a high number of viral circRNAs (Fig. 6B). As shown in Fig. 6C, the number of viral circRNAs identified from each sample was demonstrated, with a total of 77 viral circRNAs from the RSV 24-h group and a total of 1,239 viral circRNAs from the RSV 48-h group.

Next, we profiled the characteristics of viral circRNAs (Fig. 6D to G), the splicing signals of viral circRNAs were investigated, and the results showed that most (80%) of the splicing signals did not have the canonical GT/AG donor/acceptor sequence, which is different from those of the cellular circRNAs, and the dominant splicing signals were replaced by the AT/TA donor/acceptor sequence (Fig. 6D). Second, the read distributions

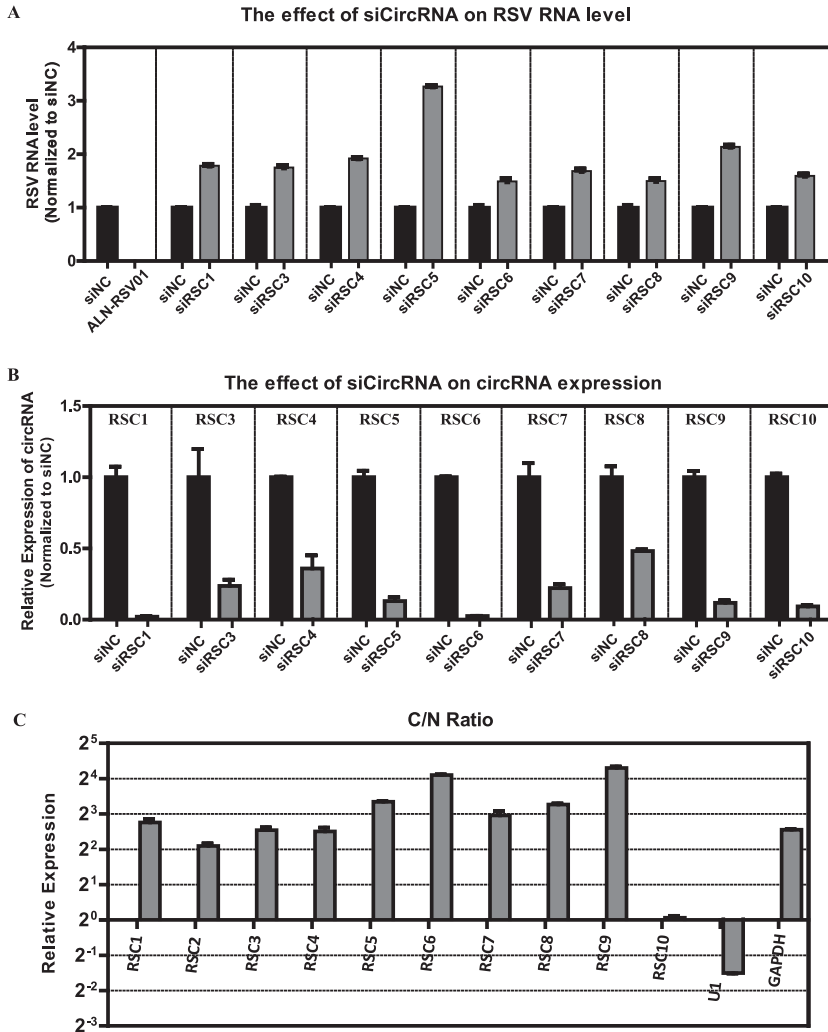


FIG 5 Analysis of the effects of the top 10 RSCs on RSV RNA levels in infected A549 cells and the subcellular localization of the 10 RSCs. (A) RSV RNA levels in infected A549 cells (MOI = 1) transfected with three pooled siRNAs for each circRNA (siCircRNA), with the exception of RSC2, assessed by qRT-PCR. (B) qRT-PCR analysis of the respective circRNAs in A549 cells treated with three pooled siRNAs as described above for panel A. In panels A and B, the RSV RNA levels or circRNA levels were normalized to the negative-control siRNA (siNC) group. (C) qRT-PCR data indicating the abundances of 10 RSCs in the subcellular localization (cytoplasm or nucleus) of A549 cells. The amounts of circRNAs were normalized to the value measured in the nucleus. C/N ratio, ratio of cytoplasm to nucleus.

of viral circRNAs were analyzed, and 997 of the 1,254 viral circRNAs contained at least two unique back-spliced reads (Fig. 6E). Third, almost all of the viral circRNAs originated from RSV gene RNA, whereas only a small number of viral circRNAs aligned with intergenes, and no viral circRNAs mapped to the leader or trailer sequences (Fig. 6F). Finally, the average and median lengths of viral circRNAs were 316 and 262 nt, respectively, and the majority of viral circRNAs were less than 500 nt (Fig. 6G).

Identification of temporally expressed clusters with 1,254 viral circRNAs and validation of the eight representative viral circRNAs.

Next, the expression of viral circRNAs in RSV-infected A549 cells was calculated, which was referenced to the cellular circRNAs' expression and also based on RPM. We also performed STEM clustering with 1,254 viral circRNAs to demonstrate the dynamic expression of RSV-derived viral circRNAs. As expected, we obtained four generally rising temporal expression clusters because the expression of viral circRNAs depended on RSV RNA replication and viral production. Two of the four clusters were significant (Fig. 7A); we named the two significant clusters of viral circRNAs the vUP1 and vUP2 clusters, which had 1,178 and 54 circRNAs, respectively. For the vUP1 and vUP2 clusters, line plots and heat maps were

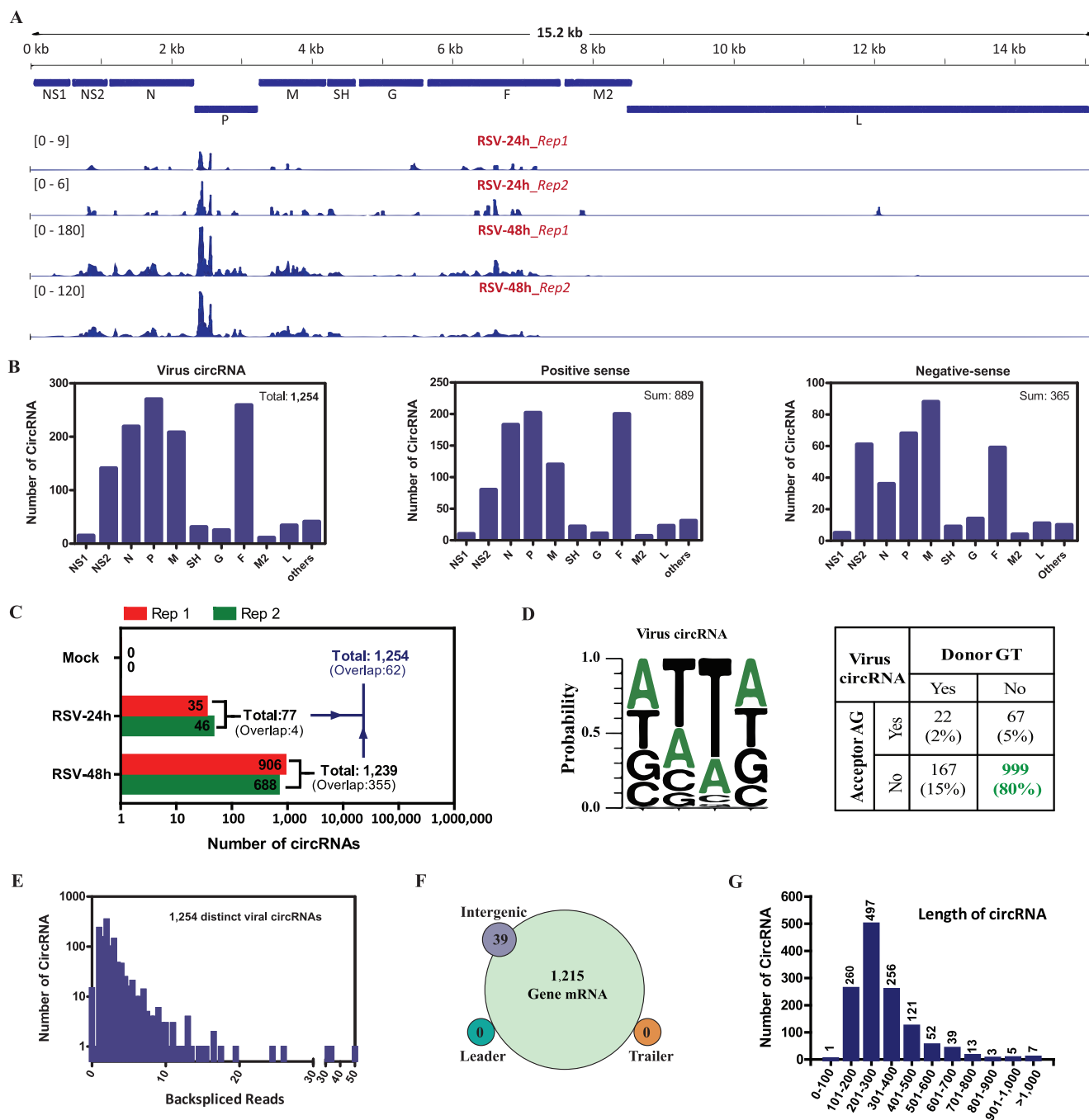


FIG 6 Profiling of viral circRNAs in RSV-infected A549 cells. (A) Integrative Genomics Viewer (IGV) displaying the coverage of candidate viral back-splice junctions aligning to the RSV genome identified in each RSV-infected sample. Standardized coverage depths (y axis) are indicated for each alignment. (B) Numbers of viral circRNAs mapped to each RSV gene, including general RSV RNA (left), positive-sense RSV RNA (middle), and negative-sense RSV RNA (right). (C) Length distribution of viral circRNAs. (D) Back-splice signals of viral circRNAs. (E) Numbers of viral circRNAs and back-spliced reads identified in all samples. (F) RSV genomic region annotations and numbers of viral circRNAs. (G) Length distribution of viral circRNAs.

used to demonstrate fold changes and \log_2 expression ratios of RPM, respectively; four representative viral circRNAs from each cluster are listed in the bottom panels, that is, *rsv_circ_449/482/664/969* from the vUP1 cluster and *rsv_circ_305/443/526/561* from the vUP2 cluster (Fig. 7A).

We next analyzed the eight viral circRNAs from the vUP1 and vUP2 clusters. Detailed characteristics of the eight viral circRNAs are shown in Table 2. Divergent primers were designed against the eight viral circRNA candidates, each primer pair amplified a single and distinct product of the expected size from RSV-infected A549 cells (Fig. S5A), and the

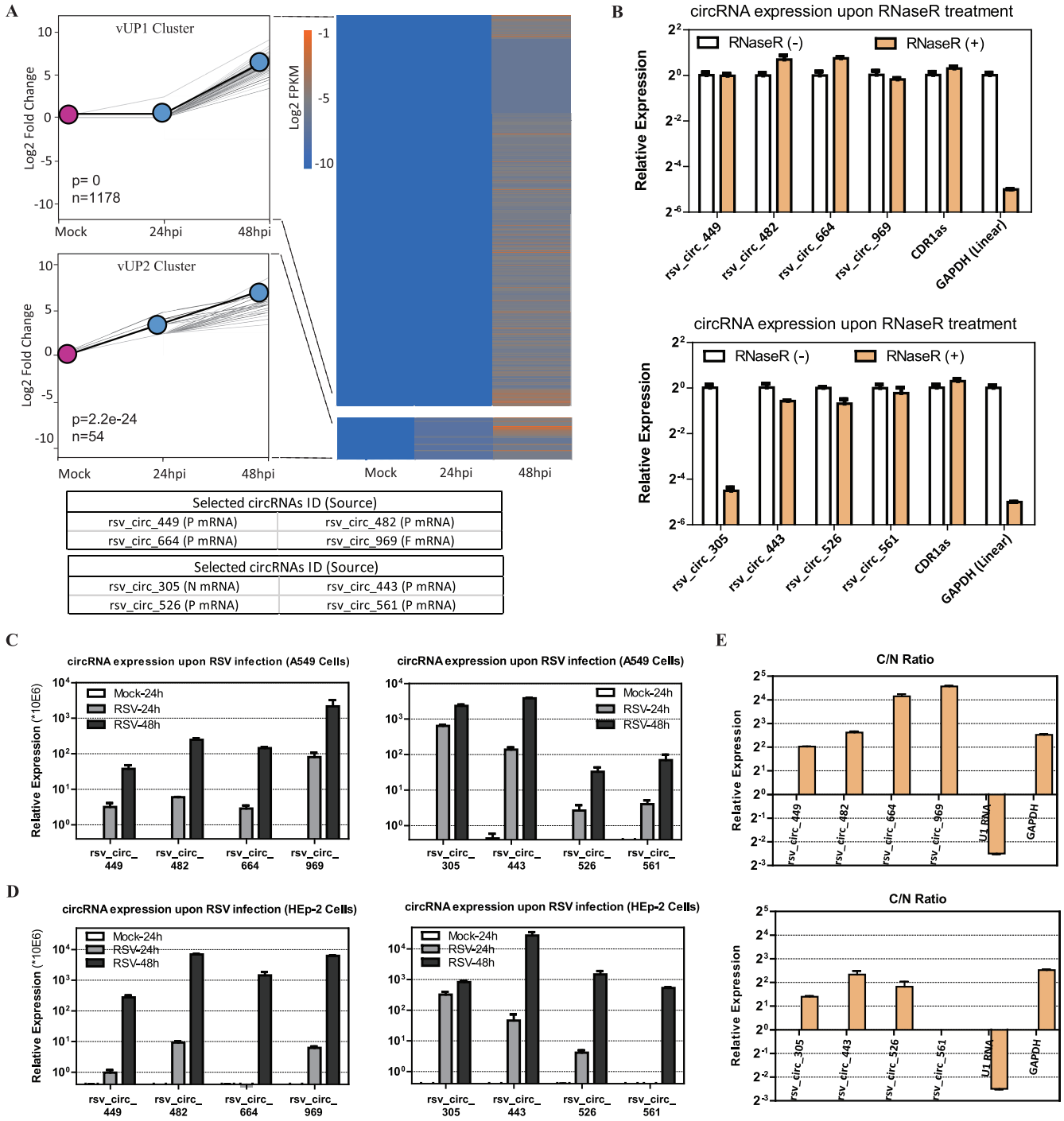


FIG 7 Trend analysis of viral circRNAs upon RSV infection and validation of the eight representative viral circRNAs from the vUP1 and vUP2 clusters. (A) Results showing two significant temporal clusters ($P < 0.05$) by STEM analysis. (Left) Line plots were used to show fold changes (the number of circRNAs assigned to each cluster and P values are shown). The gray lines indicate profiles of the individual circRNAs, and the black lines show the model profile for each cluster in the line plots. (Right) Heat map for viral circRNAs from the vUP1 and vUP2 clusters based on RPM of RNA-seq data (\log_2 scale). (Bottom) Representative circRNAs with the source of viral genes in parentheses for each cluster. (B) qRT-PCR analysis of the abundances of the eight viral circRNAs treated with RNase R. The amounts were normalized to the value measured in the untreated group. (C) Validation of the eight viral circRNAs' upregulation upon RSV infection in A549 cells (MOI = 1) by qRT-PCR analysis. (D) Validation of the eight viral circRNAs' upregulation upon RSV infection in HEp-2 cells (MOI = 1) by qRT-PCR analysis. In panels C and D, the amounts were normalized to the value measured in the mock infection group. (E) qRT-PCR data indicating the abundances of the eight viral circRNAs in the subcellular localization (cytoplasm or nucleus) of A549 cells. C/N ratio, ratio of cytoplasm to nucleus. In panels B to E, data are presented as means \pm SEMs ($n = 3$).

back-splicing junctions of the eight viral circRNAs were further validated by Sanger sequencing (Fig. S5B). The enrichment of seven out of eight back-spliced events was apparent following RNase R treatment (Fig. 7B); however, the expression of *rsv_circ_305* was significantly decreased upon RNase R treatment (Fig. 7B). Quantitative PCR (qPCR) validation has shown that some experimentally validated circRNAs are sensitive to RNase R (23, 29–31); it is unclear whether there are specific features or structures of these circRNAs that systematically result in RNase R sensitivity (32).

We then validated the expression trend of viral circRNAs upon RSV infection in A549 cells (MOI = 1) by qRT-PCR (Fig. 7C). Furthermore, we investigated the expression trends of the eight viral circRNAs upon RSV infection in HEp-2 cells (MOI = 1) (Fig. 7D). The qRT-PCR results showed that all eight viral circRNAs were significantly increased in RSV-infected A549 and HEp-2 cells (Fig. 7C and D). Subcellular localization analysis of the eight viral circRNAs was also performed, and the results showed that seven of the eight viral circRNAs accumulated in the cytoplasm, while only *rsv_circ_561* accumulated in both the cytoplasm and nucleus (Fig. 7E).

Given that some viral circRNAs are derived from the RSV negative-sense genome and that some viral circRNAs are derived from the positive-sense antigenome or positive-sense mRNA, circRNA-specific reverse transcription primers were designed against *rsv_circ_969* and *rsv_circ_443*, respectively (Table S1A) to verify that *rsv_circ_969* is from positive-sense RNA/mRNA and that *rsv_circ_443* is from negative-sense RNA. As illustrated in Fig. S6, *rsv_circ_969* is predicted to be derived from positive-sense RSV F gene RNA/mRNA, which has an AA/AT donor/acceptor sequence, and *rsv_circ_443* is predicted to be derived from negative-sense RSV P gene RNA, which has an AT/TA donor/acceptor sequence. The RT-PCR results with *rsv_circ_969*- or *rsv_circ_443*-specific reverse transcription primers showed that a single and distinct product of the expected size from RSV-infected A549 cells was amplified with each primer pair compared with mock-infected A549 cells, and the expected products were further validated by Sanger sequencing (data not shown).

DISCUSSION

This study is the first to characterize the cellular and viral circRNAomes induced by RSV infection in A549 cells, which is a widely used *in vitro* model of RSV infection of airway epithelial cells. First, from the perspective of the cellular circRNAome, we identified a large number of cellular circRNAs in RSV- and mock-infected A549 cells from diverse genomic locations. Filtering analysis identified 2,280 differentially expressed cellular circRNAs, and further STEM trend clustering with these differentially expressed circRNAs identified three significant expression clusters (UP1, UP2, and UP3) that exhibited generally rising trends upon RSV infection. Subsequent GO process and KEGG pathway enrichment analyses with parental source genes of 1,089 circRNAs from the three significant clusters revealed the most significant regulated GO processes and KEGG pathways. The actual existence of the top 10 RSCs from the focused UP1 cluster was validated by RT-PCR, Sanger sequencing, and RNase R resistance. Next, the increased expression of the 10 RSCs by RSV infection in A549 cells was validated by qRT-PCR; further results showed that pIC and VSV also induced the upregulation of the 10 RSCs. The siRNA results indicated that the concerned RSCs from the UP1 cluster generally inhibited RSV replication. Second, from the perspective of the viral circRNAome, we identified 1,254 viral circRNAs in RSV-infected A549 cells. As expected, STEM trend analysis with viral circRNAs demonstrated two significant clusters (vUP1 and vUP2). The actual existence of eight representative viral circRNAs from the vUP1 and vUP2 clusters was also validated with the same assays as those for cellular circRNAs, that is, single RT-PCR products, Sanger sequencing, and RNase R resistance. The expression of the eight circRNAs induced by RSV infection was validated by qRT-PCR in A549 cells and HEp-2 cells. Additionally, we confirmed that *rsv_circ_969* in the vUP1 cluster is positive sense and that *rsv_circ_443* in the vUP2 cluster is negative sense.

circRNAs are found across every domain of life, and they have been identified and characterized from archaea (33), plants (34), and animals (6). For viruses, DNA viruses,

including EBV, KSHV, and HPV, were reported to express viral circRNAs recently (16–19). The present study further expands our contention that circular RNAs could be derived from an RNA virus, RSV. We identified 53,719 cellular circRNAs from the human genome (3.3 Gb long) and 1,254 viral circRNAs from the RSV RNA genome (15.2 kb long). It appears that the smaller RSV RNA genome produces more circRNAs per kilobase of genome length than the human genome. We further profiled the characteristics of cellular and viral circRNAs. First, from the perspective of genomic locations, our findings showed that the majority of cellular circRNAs were derived from exon circularization and that the majority of viral circRNAs were derived from RSV gene mRNA, both of which cover the open reading frame (ORF). Second, from the perspective of circRNA length, our results showed that the average and median lengths of cellular circRNAs (2,386 nt and 637 nt, respectively) (see Fig. S1C in the supplemental material) were longer than those of the viral circRNAs (316 nt and 262 nt, respectively) (Fig. 6G). Finally, the splicing signals were analyzed. Most reported circRNAs from eukaryotic cells are generated in a spliceosome-dependent manner (9), whereas the circularization process is independent of spliceosomes in archaea (33). Our results demonstrated that cellular circRNAs had a canonical GT/AG splicing donor/acceptor sequence (Fig. 2C), whereas viral circRNA had a flanking AT/TA donor/acceptor sequence but not a canonical GT/AG splicing sequence (Fig. 6D), which suggests that viral circRNAs of RSV formed by a mechanism that is independent of spliceosomes. RSV genome transcription and replication occur in the cytoplasm, and previous observations showed that RSV can grow even without nuclear involvement (1) and, however, that spliceosome-dependent splicing was in the nucleus; these observations also support the above-mentioned assumption that viral circRNAs of RSV formed not depending on spliceosomes.

We performed RNA pulldown assays coupled with mass spectrometry (MS) to elucidate the biogenesis mechanism of these viral circRNAs. It is known that RSV infection induces the formation of spherical cytoplasmic granules called inclusion bodies (IBs), which have been revealed to be viral factories where viral RNA synthesis (i.e., replication and transcription) occurs. RSV RNA synthesis is performed by the viral RNA-dependent RNA polymerase (RdRp), which is a complex of at least two proteins, the catalytic core L and the cofactor P. Several cellular proteins (such as heat shock protein 70/90 [HSP70/90] [35, 36] and actin [37]) proposed to be involved in the synthesis of RSV RNA were shown to colocalize within IBs (38). Interestingly, our MS results showed that the viral polymerase L was present in the viral circRNA-bound protein complex, and multiple HSP70s/HSP90s and actin were also present in the above-mentioned protein complex (data not shown). Based on these results, we hypothesized that viral proteins and assistant cellular proteins that participated in RSV RNA synthesis are also involved in the production of viral circRNAs. Inspired by this hypothesis, we further analyzed the flanking sequences of RSV mRNAs (Fig. S7A) (1), which were also synthesized by the viral RdRp. To our surprise, the dominant donor/acceptor-like flanking signals of RSV mRNAs were also the AT/TA sequences (Fig. S7A and B), and the probability summary of flanking signals between RSV mRNAs and viral circRNAs showed that they were strikingly similar (Fig. S7B and C). These results suggest that there may be specific flanking sequences that are employed by the viral RdRp for viral mRNA/circRNA generation. This is an interesting finding, and we will dig into it.

In the current study, we found that RSV infection induced significant changes in cellular circRNA expression, and as demonstrated, the number of upregulated circRNAs was slightly higher than the number of downregulated circRNAs (Fig. 2D). By characterizing the dynamic changes in cellular circRNAs upon RSV infection, we identified 1,089 circRNAs with RSV-induced generally increasing expression patterns. Further results showed that both RSV and VSV infection induced the expression of the top 10 RSCs from the UP1 cluster, and pIC treatment exhibited similar inductions. Interestingly, the expressions of the 10 cellular circRNAs were all potentially regulated by IFN-related transcription factors (TFs) (interferon regulatory factor 3/7/9 [IRF3/7/9], STAT1/2, and NF- κ B) (39), as the promoters of the best-matching mRNA transcripts of the 10 cellular

circRNAs contain binding sites of IFN-related TFs predicted by AnimalTFDB3.0 (40) (Table S1B). These findings support the contention that these circRNAs are related to the antiviral response induced by RSV infection, as indicated by the GO and KEGG pathway enrichment analyses.

Subsequent investigation demonstrated that the top 10 RSCs from the UP1 cluster generally inhibited RSV replication. This result is reasonable because these circRNAs are assumed to be upregulated by the antiviral response induced by virus infection. Given that nearly all of the 10 circRNAs were abundant in the cytoplasm and that one of the most notable functions of cytoplasm circRNAs is the regulation of microRNA activity through sponging mechanisms, we mined online AGO2 photoactivatable ribonucleoside-enhanced crosslinking and immunoprecipitation (PAR-CLIP) or high-throughput sequencing of RNA isolated by crosslinking immunoprecipitation (HITS-CLIP) data from the doRiNA database (41) to determine if AGO2 occupies the region of these circRNAs. The mining results showed that 9 out of 10 circRNAs contain AGO2-binding sites and that 8 out of 10 circRNAs contain at least three AGO2-binding sites (Fig. S8). Therefore, these circRNAs possibly function by sponging microRNA. In addition, although circRNAs are believed to function mostly through noncoding mechanisms, some circRNAs have demonstrated protein-encoding capability but only when they contain ORF and internal ribosome entry site (IRES) elements (42). Xia et al. and Chen et al. developed online databases, the cancer-specific circRNA database (CSCD) (43) and circRNADb (44), respectively. The CSCD contains ORF information for 1,394,023 circRNAs from both tumor and normal samples, and circRNADb provides both IRES and ORF information for 32,914 human exonic circRNAs. We retrieved IRES and ORF information for the 10 RSCs from the two databases and found that RSC3, RSC5, RSC8, and RSC9 contain both IRESs and ORFs (Table S1B), indicating that these four circRNAs could generate translated products. Therefore, it cannot be excluded that these circRNAs function through coding proteins, but this hypothesis needs further investigation.

Although RSV was discovered more than 60 years ago, our understanding of the extent and diversity of the RSV transcriptome is limited. In this study, we report that RSV expresses a repertoire of a class of ncRNAs, namely, circRNAs. First, among the 1,254 viral circRNAs, 889 were from the positive-sense antigenome or mRNA, which is more than the 365 negative-sense circRNAs. This result is consistent with the fact that the antigenome RNA and mRNA of RSV are more abundant than genome RNA. Second, the RSV genome has 10 genes in the order 3' NS1-NS2-N-P-M-SH-G-F-M2-L, in which the encoded proteins of the N, P, M, F, and L genes have clear orthologues throughout the *Paramyxoviridae*, and their relative genome order is conserved. Our results showed that the N, P, M, F, and NS2 genes were the top five genes with a large number of viral circRNAs. These observations suggest that N, P, M, and F are important for RSV infection, but although L is the largest gene and functionally conserved throughout the *Paramyxoviridae*, the number of viral circRNAs from the L gene was very small. Third, some of the RSV-derived circRNAs were expressed at levels that are comparable to or higher than those of the majority of cellular circRNAs. This finding supports the contention regarding the potential functional role of viral circRNAs. Finally, the eight representative viral circRNAs were upregulated by RSV infection in both A549 cells and HEp-2 cells, suggesting their roles in fundamental processes during viral infection. Together, these findings reveal a spectrum of RSV circRNAs with potential functional roles in RSV infection.

Overall, we revealed a new layer of host-virus interactions with circRNAs: RSV infection induced the differential expression of cellular circRNAs, some of which affected RSV infection, and RSV could also express viral circRNAs. These cellular or viral circRNAs may be novel biomarkers or therapeutic targets.

MATERIALS AND METHODS

Library construction and RNA sequencing. After extraction, total RNAs were subjected to rRNA removal and then treated with RNase R to degrade the linear RNAs prior to library preparation. Next, a strand-specific library was constructed and sequenced using the Illumina HiSeq 2500 platform. Library

construction and RNA sequencing were performed at the Gene Denovo Biotechnology Company (Guangzhou, China).

Cell cultures and treatments. A549 cells (catalogue no. TCHu150; The Chinese Academy of Sciences Cell Bank) and HEp-2 cells (ATCC CCL-23) were grown in Ham's F-12K medium (catalogue no. 21127-022; Invitrogen) and Dulbecco's minimal essential medium (DMEM), respectively, and both media were supplemented with 10% fetal bovine serum (FBS; HyClone) and 1% penicillin-streptomycin. The cells were maintained at 37°C in a humidified atmosphere containing 5% CO₂.

pIC was purchased from Sigma (catalogue no. P9582). A549 cells were seeded into 6-well plates 16 h before treatment, and each 6-well plate then received 10 µg of pIC by transfection. Transfection was performed with 3.75 µl of Lipofectamine 3000 (Invitrogen) in 250 µl Opti-MEM medium (Gibco).

Viruses, stock preparation, and viral infections. RSV (A2 strain) was provided by Zifeng Yang (First Affiliated Hospital of Guangzhou Medical University, Guangzhou, China), and viruses were grown in HEp-2 cells for large-scale preparation. VSV was provided by Mingzhou Chen (State Key Laboratory of Virology and Modern Virology Research Center, Wuhan University), and viruses were grown in Vero cells for large-scale preparation. For viral infections, A549 or HEp-2 cells were washed with phosphate-buffered saline (PBS) and incubated with the viral inoculum in medium (2% FBS) for 90 min at 37°C at the indicated MOIs; after that time, the inoculum was removed, and fresh medium was added.

RSV titration. To determine the viral titer, HEp-2 cell monolayers were incubated with serial dilutions of the virus supernatants for 90 min at 37°C and then overlaid with medium containing 2% FBS and 1% methylcellulose. At 5 days postinfection (dpi), the cells were fixed with 10% (vol/vol) formaldehyde for 10 min, subsequently stained with 1% crystal violet for 20 min, and then washed with running water. Plaques were visualized and counted.

Preparation of cell extracts, Western blotting, and antibodies. Proteins were extracted from cells using radioimmunoprecipitation assay buffer supplemented with protease inhibitors (Sigma), with GAPDH as an internal control. For Western blotting, equal amounts of protein extracts boiled with a sodium dodecyl sulfate (SDS) loading buffer were subjected to SDS-polyacrylamide gel electrophoresis and then transferred onto a nitrocellulose membrane (Poretran). The membrane was subsequently incubated with the respective primary antibodies. Horseradish peroxidase (HRP)-conjugated secondary antibodies were used to visualize the respective proteins with an enhanced chemiluminescence detection system (Millipore). The following primary antibody was used for Western blotting: monoclonal mouse anti-RSV fusion protein antibody (catalogue no. sc-101362; Santa Cruz).

RNA preparations. Total RNA was extracted from cells using TRIzol (Invitrogen) according to the manufacturer's instructions. Nuclear and cytoplasmic RNAs were isolated using the Paris kit (catalogue no. AM1921; Invitrogen) according to the vendor's protocol.

Reverse transcription, PCR, and real-time PCR. RNA was reverse transcribed by using the PrimeScript RT reagent kit with gDNA Eraser (catalogue no. RR047A; TaKaRa) in the presence of random hexamers (TaKaRa). The cDNA was used to perform PCR or qPCR using a TB green premix ExTaq II kit (catalogue no. RR820A; TaKaRa). The primers used are listed in Table S1A in the supplemental material. The housekeeping 18S rRNA or GAPDH gene served as an internal control. All reactions were run in triplicate using the Applied Biosystems 7500 real-time PCR system.

RNase R resistance analysis. Ten micrograms of total RNA was incubated for 20 min at 37°C with or without 2 U of RNase R (catalogue no. RNR07250; Epicentre) per µg of RNA, and therefore, the total amount of RNase R for 10 µg of RNA was 20 U. The resulting RNA was then purified with an RNeasy MinElute clean-up kit (catalogue no. 74204; Qiagen).

Time series analysis to identify circRNAs across RSV infection. circRNAs by the criteria of a fold change of >2.0 or <0.5 and a *P* value of <0.05 between the two compared groups of three (mock, 24 hpi, and 48 hpi) were taken for further analysis. In total, 2,208 circRNAs were obtained for STEM clustering analysis. STEM clustering, which is specifically designed to handle short time series gene expression data, was used to find the significant temporal patterns in RSV-associated circRNAs. Significant temporal expression patterns were obtained from expression profiles of RSV-associated circRNAs at two different time points (24 hpi and 48 hpi) by assuming the mock infection sample as a base time point. The clustered patterns with *P* values of <0.05 were considered significant patterns. There were 1,089 (out of 2,208) circRNAs showing significant temporal expression patterns and 1,119 (out of 2,208) circRNAs showing nonsignificant temporal expression patterns across RSV infection, as shown in Fig. 3A to C and Fig. S2, respectively.

Bioinformatic analysis tools. circBase (21) was used to annotate the identified cellular circRNAs in A549 cells. Viral circRNAs were displayed by IGV in reference to the RSV genome (GenBank nucleotide sequence accession no. M74568.1). The GO and KEGG pathway gene annotation enrichment analyses were performed using DAVID (<https://david.ncicrf.gov/>) (25, 45). Venn diagrams were generated using an online analysis platform (<http://bioinfogp.cnb.csic.es/tools/venny/index.html>). The PCA, cluster, and trend analyses were performed using OmicShare tools (Gene Denovo).

SUPPLEMENTAL MATERIAL

Supplemental material is available online only.

TEXT S1, DOCX file, 0.04 MB.

FIG S1, PDF file, 2 MB.

FIG S2, PDF file, 2.4 MB.

FIG S3, PDF file, 1.1 MB.

FIG S4, PDF file, 1.1 MB.

FIG S5, PDF file, 1.9 MB.

FIG S6, PDF file, 1.9 MB.

FIG S7, PDF file, 0.5 MB.

FIG S8, PDF file, 0.7 MB.

TABLE S1, DOCX file, 0.04 MB.

ACKNOWLEDGMENTS

W.Y. was supported by the National Science Foundation (31500142) and the Science and Technology Program of Guangzhou (202102020088). H.C. was funded by the National Science Foundation (32000662). X.Z. was supported by the Science and Technology Program of Guangzhou (201902020001 and 201905010004).

We declare no competing interests.

REFERENCES

- Collins PL, Fearn R, Graham BS. 2013. Respiratory syncytial virus: virology, reverse genetics, and pathogenesis of disease. *Curr Top Microbiol Immunol* 372:3–38. https://doi.org/10.1007/978-3-642-38919-1_1.
- Griffiths C, Drews SJ, Marchant DJ. 2017. Respiratory syncytial virus: infection, detection, and new options for prevention and treatment. *Clin Microbiol Rev* 30:277–319. <https://doi.org/10.1128/CMR.00010-16>.
- Cockerill GS, Good JAD, Mathews N. 2019. State of the art in respiratory syncytial virus drug discovery and development. *J Med Chem* 62:3206–3227. <https://doi.org/10.1021/acs.jmedchem.8b01361>.
- Marcandalli J, Fiala B, Ols S, Perotti M, de van der Schueren W, Snijder J, Hodge E, Benhaim M, Ravichandran R, Carter L, Sheffler W, Brunner L, Lawrenz M, Dubois P, Lanzavecchia A, Sallusto F, Lee KK, Veelsler D, Correnti CE, Stewart LJ, Baker D, Lore K, Perez L, King NP. 2019. Induction of potent neutralizing antibody responses by a designed protein nanoparticle vaccine for respiratory syncytial virus. *Cell* 176:1420–1431.e17. <https://doi.org/10.1016/j.cell.2019.01.046>.
- Mazur NI, Higgins D, Nunes MC, Melero JA, Langedijk AC, Horsley N, Buchholz UJ, Openshaw PJ, McLellan JS, Englund JA, Mejias A, Karron RA, Simoes EAF, Knezevic I, Ramilo O, Piedra PA, Chu HY, Falsey AR, Nair H, Kragten-Tabatabaie L, Greenough A, Baraldi E, Papadopoulos NG, Vekemans J, Polack FP, Powell M, Satav A, Walsh EE, Stein RT, Graham BS, Bont LJ, Respiratory Syncytial Virus Network (ReSViNET) Foundation. 2018. The respiratory syncytial virus vaccine landscape: lessons from the graveyard and promising candidates. *Lancet Infect Dis* 18:e295–e311. [https://doi.org/10.1016/S1473-3099\(18\)30292-5](https://doi.org/10.1016/S1473-3099(18)30292-5).
- Memczak S, Jens M, Elefsinioti A, Torti F, Krueger J, Rybak A, Maier L, Mackowiak SD, Gregersen LH, Munschauer M, Loewer A, Ziebold U, Landthaler M, Kocks C, le Noble F, Rajewsky N. 2013. Circular RNAs are a large class of animal RNAs with regulatory potency. *Nature* 495:333–338. <https://doi.org/10.1038/nature11928>.
- Wilusz JE, Sharp PA. 2013. Molecular biology. A circuitous route to noncoding RNA. *Science* 340:440–441. <https://doi.org/10.1126/science.1238522>.
- Vo JN, Cieslik M, Zhang Y, Shukla S, Xiao L, Zhang Y, Wu Y-M, Dhanasekaran SM, Engelke CG, Cao X, Robinson DR, Nesvizhskii AI, Chinnaiyan AM. 2019. The landscape of circular RNA in cancer. *Cell* 176:869–881.e13. <https://doi.org/10.1016/j.cell.2018.12.021>.
- Li X, Yang L, Chen LL. 2018. The biogenesis, functions, and challenges of circular RNAs. *Mol Cell* 71:428–442. <https://doi.org/10.1016/j.molcel.2018.06.034>.
- Chen Y, Li C, Tan C, Liu X. 2016. Circular RNAs: a new frontier in the study of human diseases. *J Med Genet* 53:359–365. <https://doi.org/10.1136/jmedgenet-2016-103758>.
- Shi J, Hu N, Mo L, Zeng Z, Sun J, Hu Y. 2018. Deep RNA sequencing reveals a repertoire of human fibroblast circular RNAs associated with cellular responses to herpes simplex virus 1 infection. *Cell Physiol Biochem* 47:2031–2045. <https://doi.org/10.1159/000491471>.
- Tagawa T, Gao S, Koparde VN, Gonzalez M, Spouge JL, Serquina AP, Lurain K, Ramaswami R, Uldrick TS, Yarchoan R, Ziegelbauer JM. 2018. Discovery of Kaposi's sarcoma herpesvirus-encoded circular RNAs and a human antiviral circular RNA. *Proc Natl Acad Sci U S A* 115:12805–12810. <https://doi.org/10.1073/pnas.1816183115>.
- Tycowski KT, Guo YE, Lee N, Moss WN, Vallery TK, Xie M, Steitz JA. 2015. Viral noncoding RNAs: more surprises. *Genes Dev* 29:567–584. <https://doi.org/10.1101/gad.259077.115>.
- Choudhary A, Madbhagat P, Sreedharaman B, Bhardwaj V, Chande A. 2021. Circular RNA as an additional player in the conflicts between the host and the virus. *Front Immunol* 12:602006. <https://doi.org/10.3389/fimmu.2021.602006>.
- Tan KE, Lim YY. 2021. Viruses join the circular RNA world. *FEBS J* 288:4488–4502. <https://doi.org/10.1111/febs.15639>.
- Toptan T, Abere B, Nalesnik MA, Swerdlow SH, Ranganathan S, Lee N, Shair KH, Moore PS, Chang Y. 2018. Circular DNA tumor viruses make circular RNAs. *Proc Natl Acad Sci U S A* 115:E8737–E8745. <https://doi.org/10.1073/pnas.1811728115>.
- Ungerleider N, Concha M, Lin Z, Roberts C, Wang X, Cao S, Baddoo M, Moss WN, Yu Y, Seddon M, Lehman T, Tibbetts S, Renne R, Dong Y, Flemington EK. 2018. The Epstein Barr virus circRNAome. *PLoS Pathog* 14:e1007206. <https://doi.org/10.1371/journal.ppat.1007206>.
- Ungerleider NA, Tibbetts SA, Renne R, Flemington EK. 2019. Gammaherpesvirus RNAs come full circle. *mBio* 10:e00071-19. <https://doi.org/10.1128/mBio.00071-19>.
- Zhao J, Lee EE, Kim J, Yang R, Chamseddin B, Ni C, Gusho E, Xie Y, Chiang CM, Buszczak M, Zhan X, Laimins L, Wang RC. 2019. Transforming activity of an oncoprotein-encoding circular RNA from human papillomavirus. *Nat Commun* 10:2300. <https://doi.org/10.1038/s41467-019-10246-5>.
- Cai Z, Fan Y, Zhang Z, Lu C, Zhu Z, Jiang T, Shan T, Peng Y. 2021. VirusCircBase: a database of virus circular RNAs. *Brief Bioinform* 22:2182–2190. <https://doi.org/10.1093/bib/bbaa052>.
- Glazar P, Papavasiliou P, Rajewsky N. 2014. circBase: a database for circular RNAs. *RNA* 20:1666–1670. <https://doi.org/10.1261/rna.043687.113>.
- Pruitt KD, Tatusova T, Brown GR, Maglott DR. 2012. NCBI Reference Sequences (RefSeq): current status, new features and genome annotation policy. *Nucleic Acids Res* 40:D130–D135. <https://doi.org/10.1093/nar/gkr1079>.
- Guo JU, Agarwal V, Guo H, Bartel DP. 2014. Expanded identification and characterization of mammalian circular RNAs. *Genome Biol* 15:409. <https://doi.org/10.1186/s13059-014-0409-z>.
- Ernst J, Bar-Joseph Z. 2006. STEM: a tool for the analysis of short time series gene expression data. *BMC Bioinformatics* 7:191. <https://doi.org/10.1186/1471-2105-7-191>.
- Huang DW, Sherman BT, Lempicki RA. 2009. Bioinformatics enrichment tools: paths toward the comprehensive functional analysis of large gene lists. *Nucleic Acids Res* 37:1–13. <https://doi.org/10.1093/nar/gkn923>.
- Alvarez R, Elbashir S, Borland T, Toudjarska I, Hadwiger P, John M, Roehl I, Morskaya SS, Martinello R, Kahn J, Van Ranst M, Tripp RA, DeVincenzo JP, Pandey R, Maier M, Nechev L, Manoharan M, Kotlianski V, Meyers R. 2009. RNA interference-mediated silencing of the respiratory syncytial virus nucleocapsid defines a potent antiviral strategy. *Antimicrob Agents Chemother* 53:3952–3962. <https://doi.org/10.1128/AAC.00014-09>.
- DeVincenzo J, Lambkin-Williams R, Wilkinson T, Cehelsky J, Nochur S, Walsh E, Meyers R, Gollob J, Vaishnav A. 2010. A randomized, double-blind, placebo-controlled study of an RNAi-based therapy directed against respiratory syncytial virus. *Proc Natl Acad Sci U S A* 107:8800–8805. <https://doi.org/10.1073/pnas.0912186107>.
- Robinson JT, Thorvaldsdottir H, Winckler W, Guttman M, Lander ES, Getz G, Mesirov JP. 2011. Integrative genomics viewer. *Nat Biotechnol* 29:24–26. <https://doi.org/10.1038/nbt.1754>.
- Westholm JO, Miura P, Olson S, Shenker S, Joseph B, Sanfilippo P, Celniker SE, Graveley BR, Lai EC. 2014. Genome-wide analysis of drosophila circular RNAs reveals their structural and sequence properties and age-dependent

- neural accumulation. *Cell Rep* 9:1966–1980. <https://doi.org/10.1016/j.celrep.2014.10.062>.
30. Jeck WR, Sharpless NE. 2014. Detecting and characterizing circular RNAs. *Nat Biotechnol* 32:453–461. <https://doi.org/10.1038/nbt.2890>.
 31. Ryu J, Kwon D-H, Choe N, Shin S, Jeong G, Lim Y-H, Kim J, Park WJ, Kook H, Kim Y-K. 2020. Characterization of circular RNAs in vascular smooth muscle cells with vascular calcification. *Mol Ther Nucleic Acids* 19:31–41. <https://doi.org/10.1016/j.omtn.2019.11.001>.
 32. Szabo L, Salzman J. 2016. Detecting circular RNAs: bioinformatic and experimental challenges. *Nat Rev Genet* 17:679–692. <https://doi.org/10.1038/nrg.2016.114>.
 33. Danan M, Schwartz S, Edelheit S, Sorek R. 2012. Transcriptome-wide discovery of circular RNAs in Archaea. *Nucleic Acids Res* 40:3131–3142. <https://doi.org/10.1093/nar/gkr1009>.
 34. Lu T, Cui L, Zhou Y, Zhu C, Fan D, Gong H, Zhao Q, Zhou C, Zhao Y, Lu D, Luo J, Wang Y, Tian Q, Feng Q, Huang T, Han B. 2015. Transcriptome-wide investigation of circular RNAs in rice. *RNA* 21:2076–2087. <https://doi.org/10.1261/rna.052282.115>.
 35. Brown G, Rixon HW, Steel J, McDonald TP, Pitt AR, Graham S, Sugrue RJ. 2005. Evidence for an association between heat shock protein 70 and the respiratory syncytial virus polymerase complex within lipid-raft membranes during virus infection. *Virology* 338:69–80. <https://doi.org/10.1016/j.virol.2005.05.004>.
 36. Munday DC, Wu W, Smith N, Fix J, Noton SL, Galloux M, Touzelet O, Armstrong SD, Dawson JM, Aljabr W, Easton AJ, Rameix-Welti MA, de Oliveira AP, Simabuco FM, Ventura AM, Hughes DJ, Barr JN, Fearn R, Digard P, Eleouet JF, Hiscox JA. 2015. Interactome analysis of the human respiratory syncytial virus RNA polymerase complex identifies protein chaperones as important cofactors that promote L-protein stability and RNA synthesis. *J Virol* 89:917–930. <https://doi.org/10.1128/JVI.01783-14>.
 37. Harpen M, Barik T, Musiyenko A, Barik S. 2009. Mutational analysis reveals a noncontractile but interactive role of actin and profilin in viral RNA-dependent RNA synthesis. *J Virol* 83:10869–10876. <https://doi.org/10.1128/JVI.01271-09>.
 38. Galloux M, Risse-Ballester J, Richard CA, Fix J, Rameix-Welti MA, Eleouet JF. 2020. Minimal elements required for the formation of respiratory syncytial virus cytoplasmic inclusion bodies in vivo and in vitro. *mBio* 11:e01202-20. <https://doi.org/10.1128/mBio.01202-20>.
 39. Schneider WM, Chevillotte MD, Rice CM. 2014. Interferon-stimulated genes: a complex web of host defenses. *Annu Rev Immunol* 32:513–545. <https://doi.org/10.1146/annurev-immunol-032713-120231>.
 40. Hu H, Miao YR, Jia LH, Yu QY, Zhang Q, Guo AY. 2019. AnimalTFDB 3.0: a comprehensive resource for annotation and prediction of animal transcription factors. *Nucleic Acids Res* 47:D33–D38. <https://doi.org/10.1093/nar/gky822>.
 41. Blin K, Dieterich C, Wurmus R, Rajewsky N, Landthaler M, Akalin A. 2015. DoRiNA 2.0—upgrading the doRiNA database of RNA interactions in post-transcriptional regulation. *Nucleic Acids Res* 43:D160–D167. <https://doi.org/10.1093/nar/gku1180>.
 42. Chen CY, Sarnow P. 1995. Initiation of protein synthesis by the eukaryotic translational apparatus on circular RNAs. *Science* 268:415–417. <https://doi.org/10.1126/science.7536344>.
 43. Xia S, Feng J, Chen K, Ma Y, Gong J, Cai F, Jin Y, Gao Y, Xia L, Chang H, Wei L, Han L, He C. 2018. CSCD: a database for cancer-specific circular RNAs. *Nucleic Acids Res* 46:D925–D929. <https://doi.org/10.1093/nar/gkx863>.
 44. Chen X, Han P, Zhou T, Guo X, Song X, Li Y. 2016. circRNADb: a comprehensive database for human circular RNAs with protein-coding annotations. *Sci Rep* 6:34985. <https://doi.org/10.1038/srep34985>.
 45. Huang DW, Sherman BT, Lempicki RA. 2009. Systematic and integrative analysis of large gene lists using DAVID bioinformatics resources. *Nat Protoc* 4:44–57. <https://doi.org/10.1038/nprot.2008.211>.